TÜBİTAK

Turk J Elec Eng & Comp Sci, Vol.18, No.5, 2010, © TÜBİTAK
doi:10.3906/elk-0906-44

Analysis and estimation of motion transmission errors of a timing belt drive

Ergin KILIÇ, Melik DÖLEN, Ahmet Buğra KOKU
Department of Mechanical Engineering, Middle East Technical University, Ankara, 06531-TURKEY
e-mail: kergin@metu.edu.tr, dolen@metu.edu.tr, kbugra@metu.edu.tr

Abstract

This paper focuses on viable position estimation schemes for timing belt drives where the position of the carriage (load) is to be determined via reference models receiving input from a position sensor attached to the actuator of the timing belt. A detailed analysis of the transmission error sources is presented, and a number of relevant mathematical models are developed using a priori knowledge of the process. This paper demonstrates that such schemes are very effective when the drive system is not subjected to external loads and operating conditions do not change considerably i.e. ambient temperature, belt tension.

Key Words: *Timing belts, error estimation, indirect measurement, accuracy enhancement.*

1. Introduction

Timing belt drives are increasingly utilized to convert rotary motion into translation in high-precision motion-control systems e.g. inkjet printers, plotters, specialized CNC machine tools, filament winding machines, rapid prototyping machines, vision systems, and some bio-medical equipment [1]. In such machines, the carriage which houses a special apparatus is usually driven by an elastic transmission element e.g. timing belt. Thus, the linear motion of the apparatus must be controlled accurately via direct position measurements so as to attain the goals of the particular task at hand.

The main disadvantage of elastic elements in such arrangements is that they introduce well-known non-linearities i.e. friction, elasticity, backlash, time delay, to the servo loop [2]. Therefore, in order to achieve the desired precision and positioning accuracy, advanced control schemes [1-6] accompany direct measurement/feedback techniques frequently. It is critical to note that when the characteristic travel-span/stroke of a generic machine is very long (> 0.5 m); the use of direct measurement techniques which includes traditional sensors i.e. potentiometers, LVDTs, linear scales, laser interferometers leads to both bulky and relatively expensive solutions. Hence, the main motivation of this paper is to propose feasible estimation schemes that use

the information emanating from a low-cost sensor on the pulley of the drive so that the position of the carriage can be estimated to the desired accuracy for "not-so-demanding" applications.

It is critical to note that such a paradigm requires a good model for the transmission errors (TEs) of timing belt mechanisms. Despite the fact that the definition of TE along with the corresponding measurement and evaluation techniques is well-known in gear (dynamics) literature [7], there are only a handful of studies that focus on the TE characteristics of timing belt drives alone. For instance, Kagotani et al. [8] present a brief overview of the relevant literature in this field. Their study investigates the transmission errors of helical timing belts over a period of one pitch of the pulley both theoretically and experimentally.

The rest of the paper is organized as follows. After this brief introduction, The system is modeled mathematically and simulation results are presented. Next, the experimental setup is described. Then, some experiments made to investigate the transmission characteristics of a generic timing belt drive is reported. Based on the data collected, this paper makes a detailed analysis of the source of position errors. Upon these results kinematic models are presented in the following section. The next article evaluates the estimation performance of the proposed models. Finally, the paper is concluded with the key points of the study.

2. Mathematical modeling and simulation

Figure1 illustrates the mathematical model of the linear guided carriage system. In that system, the motion of the motor is transmitted to the carriage via timing belt mechanism. There must be an enough clearance between the meshing teeth to ensure smooth motion without interlocking.

This backlash in the mechanism results in hysteresis phenomenon. There are many studies utilizing the Preisach model to describe the hysteretic effects encountered in various disciplines. An elementary hysteresis operator is purely defined by the Preisach model as

$$f(t) = \iint_{\alpha \geq \beta} \mu(\alpha, \beta)\, \gamma_{\alpha\beta}\, u(t)\, d\alpha\, d\beta \tag{1}$$

where α and β correspond to up- and down switching value of the hysteresis band. Similarly, $\gamma_{\alpha\beta}$ indicates each unique hysteresis elements in the system where as $\mu(\alpha, \beta)$ is an arbitrary weight function which must be defined for each system [9]. Note that the Preisach model is the most famous one among other hysteresis models. However, it will not be considered in this study owing to the fact that the Preisach model exhibits non-local memory. That is, the current value of the output does not depend on only the current value of the input but also the past extremum values of the input. It is quite possible that two outputs coincide at time t_0 but results in completely different outputs $v_1(t)$ and $v_2(t)$ for $t > t_0$ hence they exposure to the same input $u(t)$ for $t > t_0$ [10]. Another problem of this model is to determine the weight function. Experiments must be done on the system to determine this function. Moreover, equation (1) is a double integral equation. Its numerical implementation must be realized to use them in control system algorithms [11].

There are two dynamic cases in the mathematical model: first one model the upper and lower hysteresis band as the system moves in a certain direction without interrupt and the latter one models the transient region when the carriage changes its motion direction. Also, Figure 1 shows the forces occurred in the timing belt.

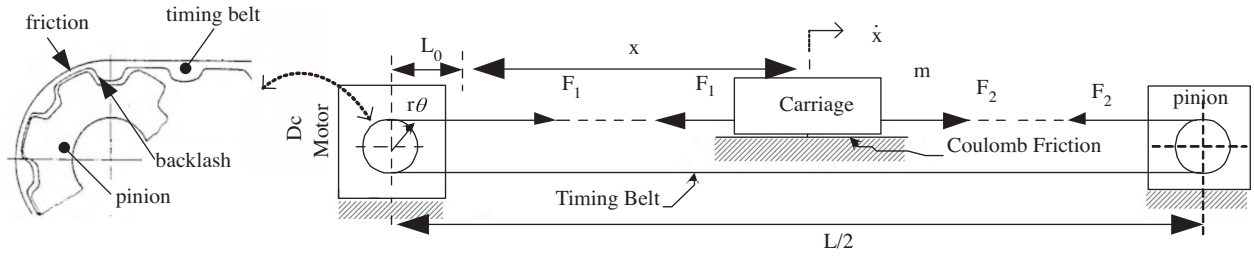

Figure 1. Free body diagram of the linear guided carriage system.

If the friction on the bearings of the pinion attached to the motor is neglected, the carriage will be actuated by the difference of the forces created in the timing belt. The free body diagram of the carriage is described in Figure 2

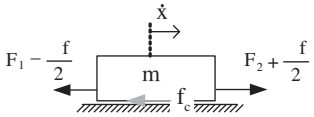

Figure 2. Free body diagram of the carriage.

Thus, the equation of the motion of the Carriage may be written

$$m\,\ddot{x} + f_c\,sgn(\dot{x}) = F_2 - F_1 + \Delta f \tag{2}$$

where f_c stands for the Coulomb friction in the bearings of the Carriage. There will be an elastic deformation due to the contact between the timing belt and the pinion teeth. As a result, this creates an additional tension force difference (Δf) on the timing belt which may be written as;

$$\Delta f = \left\{ \begin{array}{cc} k\,(r\theta - x - h), & r\theta - x \geq h \\ k\,(r\theta - x + h), & r\theta - x \leq -h \\ 0, & |r\theta - x| < h \end{array} \right\} \tag{3}$$

In (3), h (>0) $[\mu\mathrm{m}]$ refers to gap/backlash between teeth of the timing belt and the pinion; $k$corresponds to overall rigidity of the teeth. In this model, forces are created by the elastic deformation between the timing belt's teeth and the pinion's teeth. A possible configuration of this model is that the teeth are disengaged, the carriage changes its motion direction, and the timing belt teeth enter backlash region. Force is transmitted through only frictional forces developed between the pinion and belt. This phenomenon continues i.e. slippage until the backlash is closed between the pinion and timing belt teeth. The tensile forces on both sides of the timing belt become;

$$\begin{aligned} F_1 &= \bar{F} - \Delta F_1 \\ F_2 &= \bar{F} + \Delta F_2 \end{aligned} \tag{4}$$

Here, $\overline{F} > 0$ refers to the preload/tension on the belt. By definition, the perturbation forces (ΔF_1 and ΔF_2) on the belt are all non-negative quantities and less than the preload $\left(\overline{F}\right)$ itself to ensure the load-carrying capability of the belt. The Euler equation yields the relation between the tensile belt forces as [6]

$$\gamma \equiv \frac{F_2}{F_1} = \frac{\bar{F} + \Delta F_2}{\bar{F} - \Delta F_1} = e^{\mu(u)\alpha} \tag{5}$$

where α is the winding (engagement) angle of the belt (in this case, multiples of π); $\mu(u)$ stands for the "kinetic" friction coefficient which depends on the relative circumferential speed between the pinion and the belt; and u is the slip velocity. The compatibility condition requires that the change in length (extension) of the belt on one side must match with the change in length (contraction) on the other side (or vice versa) because there should be no (net) change in the length of belt, that is

$$\frac{\Delta F_2 (L - L_0 - x)}{AE} = \frac{\Delta F_1 (L_0 + x)}{AE} \tag{6}$$

where AE (in units of Newtons) is the rigidity of the cable. Using equations (4), (5) and (6) dynamic forces may be computed as;

$$\Delta F_1 = \frac{\bar{F}\,(\gamma - 1)\,(L - L_o - x)}{L_o + x + \gamma(L - L_o - x)} \tag{7}$$

$$\Delta F_2 = \frac{\bar{F}\,(\gamma - 1)\,(L_o + x)}{L_o + x + \gamma\,(L - L_o - x)} \tag{8}$$

Then, eqn. (4) becomes

$$\Delta F_1 + \Delta F_2 = \frac{\bar{F}\,(\gamma - 1)\,(L - L_o - x + L_o + x)}{L_o + x + \gamma\,(L - L_o - x)} \tag{9}$$

Thus, dynamic system may be described by the equation

$$m\,\ddot{x} + f_c\,sgn\left(\dot{x}\right) = \frac{\bar{F}\,(\gamma - 1)\,L}{L_o + x + \gamma\,(L - L_o - x)} \tag{10}$$

Note that in (10), the translation of the carriage center (x) is the input (forcing) function of this ordinary differential equation. To compute γ in (5), an advanced friction model, which considers micro-slip to a certain extent, is used. In this study, LuGre model, which has been successfully adapted by various studies [12-15], is selected for this purpose. The model in its simplest form is expressed as

$$\mu(u) = \sigma_0 z + \sigma_1 \dot{z} + \sigma_2 u \text{ where } \dot{z} = u - \frac{\sigma_0 |u| z}{\mu_k + (\mu_s - \mu_k) \exp\left[-\left|\frac{u}{v_s}\right|^a\right]} \tag{11}$$

where a, σ_0, σ_1, σ_2 are the model coefficients; z is n internal state representing average deflection of the bristles on the contacting surfaces; v_s stands for the Streibeck velocity; μ_k and μ_s denote the kinetic and static friction coefficients respectively. When the longitudinal oscillation of the timing belt is neglected, a simple kinematic analysis explains the relative velocity between the pinion and the belt:

$$u = R\dot{\theta} - \dot{x} - \rho\,\dot{\theta}\cos(\theta + \theta_0) \tag{12}$$

where ρ refers to the eccentricity of the pinion and θ_o represents the initial angle of the pinion.

Based upon these equations a numerical solution is sought. Figure 3 and Figure 4 show the input and output of the model respectively. In Figure 4, another model output is represented corresponding to a situation that there is no friction phenomena anymore between the pinion and belt when they met. So, Model 1 corresponds to a damped structure and Model 2 corresponds to an undamped structure.

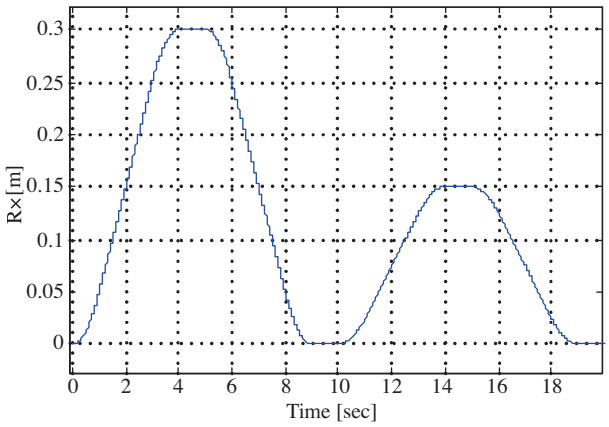

Figure 3. Input of the model.

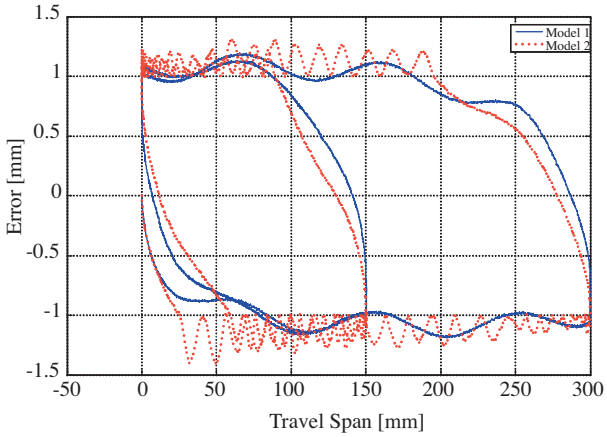

Figure 4. Output of the model.

3. Test setup

To study transmission error characteristics of a generic timing belt drive, the linear stage of a CMM has been adapted. Figure 5 describes this setup where a DC motor with a built-in gearbox drives the carriage via a timing belt. A schematic of this setup is also given in Figure 6 while Table 1 tabulates important technical data of elements used in the arrangement.

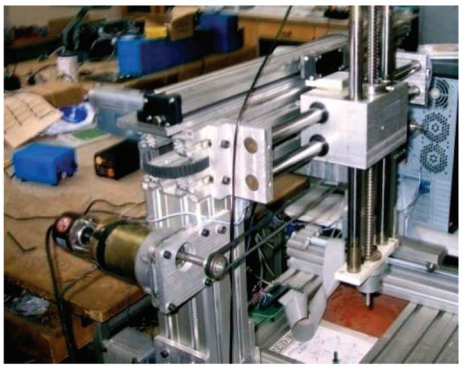

Figure 5. Photograph showing a general view of the test setup.

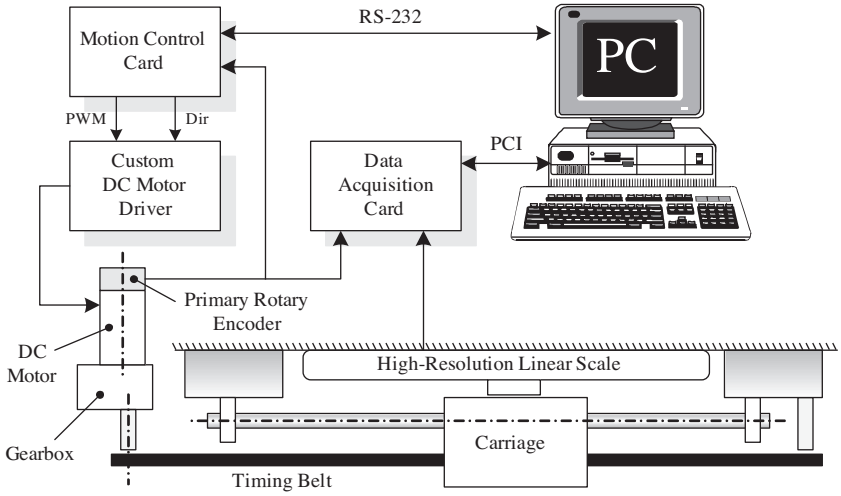

Figure 6. Schematic block diagram of the experimental setup.

Table 1. The technical data of elements of the experimental setup.

Elements	**Type / Model**	**Remarks**
Motor	150 W Brush-type DC motor	Built-in gearbox (23.7222:1)
Motor Driver	Trans-conductance amplifier	800 W / MOSFET
Timing Belt	General purpose	Pitch: 5.08 mm (0.2")
Controller	PIC16F877A @ 20 MHz	8-bit RISC controller
Motor Encoder	Autonics ENB quadrature optical encoder	2000 pulses/rev (ea. quad. channel)
Linear Scale	Heidenhain LS-176C (Distance coded)	500 pulses / mm (ea. quad. channel)
Data Acquisition Board	Humusoft MF-614	4 enc. inputs, 4 DAC, 16 ADC, 8 DI, 8 DO.
Software	Matlab Real-time Windows Target	Data capture, analysis, and visualization

A high resolution linear scale (LS) is integrated into the setup to help modeling and to verify the estimation performance of the proposed models. Notice that in this setup, it is desirable to control the acceleration / deceleration of the carriage accurately; so a custom motion controller is used in the system.

In order to determine the displacement errors introduced by the transmission system, the position measurements of the primary encoder (PE) is compared with those of the high-resolution linear scale that is directly coupled to the carriage of the linear stage. However, the measurement axes of the LS and that of the PE does not coincide due to the limitations imposed by the physical layout of the stage. Therefore the Abbe offset errors will be indirectly included to the observed displacement errors; see Figure 7. The elements of the system have several shortcomings, there are several hard- and soft-nonlinearities associated with these elements; backlash (gearbox + timing belt), time delay (timing belt), friction (bearings), visco-elastic behavior of the belt, and more. Thus, estimation of the position of the carriage by using indirect measurement techniques proves to be quite challenging and demands extensive modeling efforts.

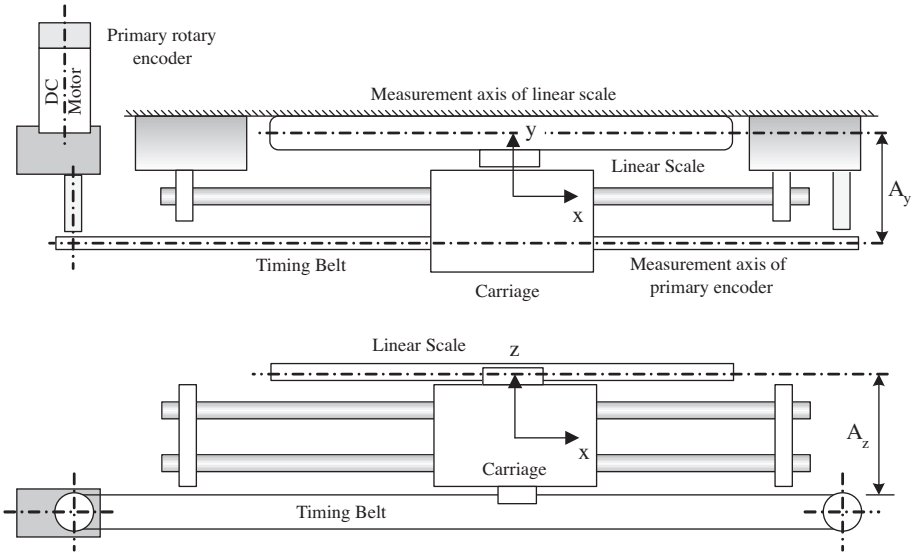

Figure 7 Abbe offsets.

The difference between the measurements takes the following form by the transmission system:

$$\Delta x = x_{LS} - x_{PE} = \delta_x(x_{PE}) + A_z\varepsilon_y(x_{PE}) - A_y\varepsilon_z(x_{PE}) \tag{13}$$

where x_{LS} and x_{PE} refer to the position measurements of the LS and PE respectively. Here, A_y and A_z indicates the value of Abbe offsets. Moreover, ε_y and ε_z are the small angular rotations about principal axes and δ_x is the displacement error introduced by the transmission system. Since Δx in (13) constitutes the geometric/kinematics errors associated with support elements i.e. anti-friction bearings, bearing shafts; the transmission error, has to be isolated via relevant transformations. Figure 8 describes such displacement errors and angular rotations about principal axes of this CMM.

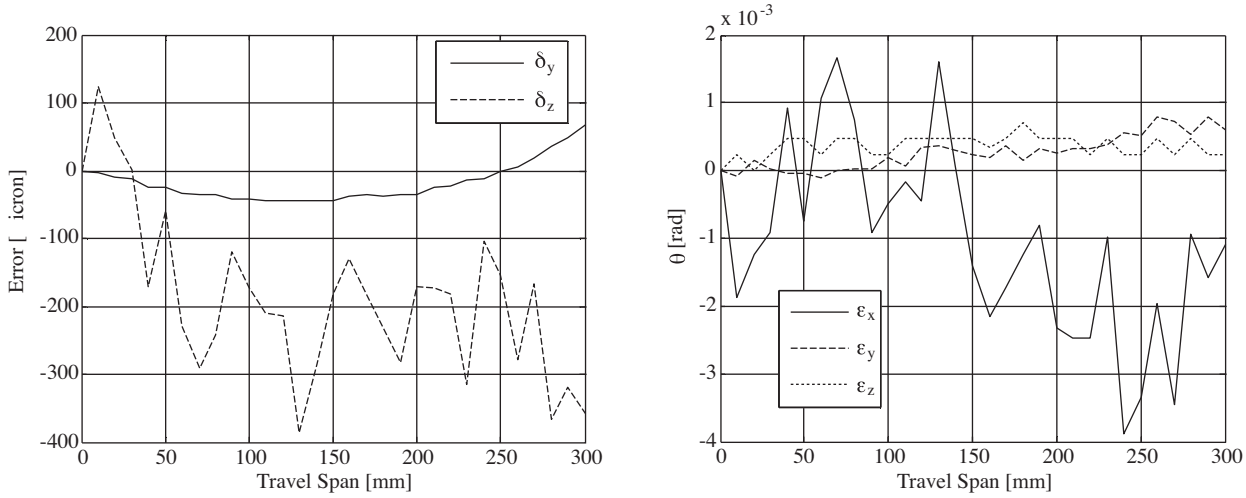

Figure 8. Plots show Displacement errors and Angular rotations about principal the axes.

4. Experiments

Throughout this study, several tests are conducted. First, the repeatability of the motion is studied as a prerequisite to devise reliable reference models. In all these tests , the motor's velocity which is controlled along a trapezoidal path accurately is shown in Figure 9 and the resulting position/ tracking error in Figure 10 (that essentially go to zero at the steady state) may be assumed low for all practical purposes. Under these conditions, the positioning error patterns ($\Delta x = x_{LS}$ - x_{PE}) for twelve different trajectories overlaid are printed in Figure 11. As it may be verified by the frequency chart in Figure 12, the positioning errors exhibit hysteresis characteristics, and they are quite repeatable. This property suggests the development of advanced estimator models [16].

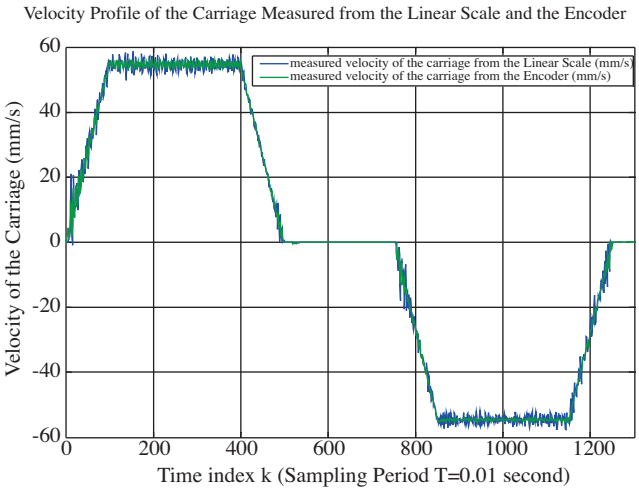

Figure 9. Velocity profile of the carriage.

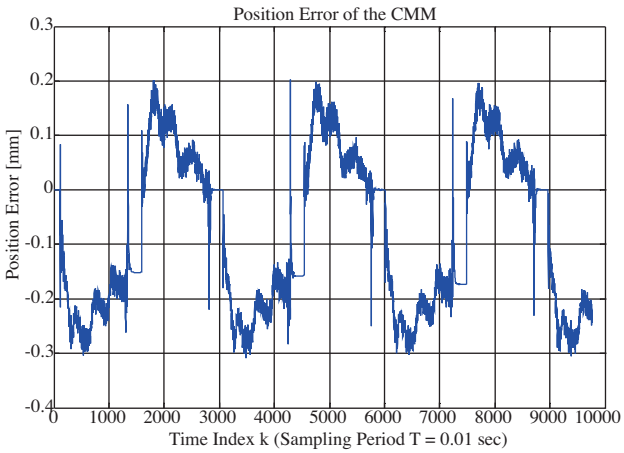

Figure 10. Position tracking error.

Positioning error data of carriage is collected then they are conditioned by a low-pass filter to eliminate the high-frequency harmonics introduced by the transmission system (gearbox + timing belt). In fact, the close examination of the error patterns in Figure 11 reveals critical points about the properties of the system under investigation:

- Hysteresis band, which is roughly 0.3 mm for the test cases, is apparently a consequence of the backlash between the timing belt and the driving pinion. A dramatic increase in the belt tension tends to widen this band as the gap between the teeth gets stretched out.

- As it is mentioned earlier, the Abbe offset errors manifest themselves as the waveforms on the upper and lower boundaries. Hence, mechanical manipulations of the bearing elements usually exhibit a different texture on these bounds.

- A fundamental harmonic component whose magnitude with 10 microns is superimposed onto the band and its frequency is equal to the tooth-passing frequency of the belt and hence these variations can be attributed to form errors of the belt.

- Harmonics which are induced by the two-stage gearbox of the motor appear to be quite negligible whereas the transition in the backlash zone whose bandwidth is 0.12 mm is extremely fast when the carriage changes its motion direction.

The next set of experiments focuses on the effect of velocity on the transmission error. Figure 13 illustrates five different displacement errors along full travel span of the mechanism. As it can be seen from the Figure, dramatic changes in steady-state velocity have only minor influences on the nature of the nonlinear relationship.

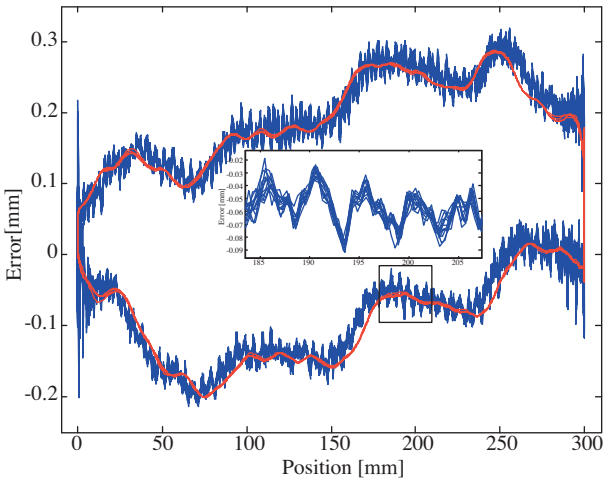

Figure 11. Position errors for 12 cases.

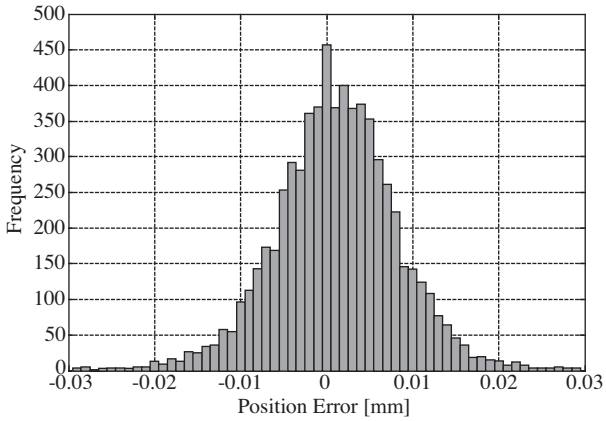

Figure 12. Frequency of errors.

Finally, the effect of inertial forces is investigated by changing the acceleration and deceleration profile of the motor such that the sliding motion inside the hysteresis band is induced. As it can be seen from Figure 14, the inertial forces do not have a considerable effect on the closing distances. Similarly, Figure 15 elaborates the closing distances when the direction of motion is reversed at various intermediate locations. It is interesting to note that when the motion direction is reversed, the power transmitting teeth disengage and micro-slip under external excitation dominates. As a consequence of this phenomenon, the belt slowly slides until the next set of teeth pairs engage into transmission. There are few efforts to develop dynamic models that explain this phenomenon satisfactorily and development of such advanced models is an active research field in tribology [17].

5. Kinematic models of timing belt mechanism

Despite their common use in precision machinery, the transmission characteristics of elastic transmission elements have not been fully evaluated in the literature. Hence, a simple but effective kinematic model is to be devised in this study. Unfortunately, the trajectories being followed inside the band can be quite complicated owing to the fact that the micro-slip process becomes dominant in the region and it cannot be described satisfactorily. Therefore, instead of developing sophisticated dynamic models with a large number of free parameters; a more pragmatic approach is to be followed in this paper. In fact, the trajectories presented in Figure 15 suggest the development of three different models with different physical meanings and computational costs. These models are explained next.

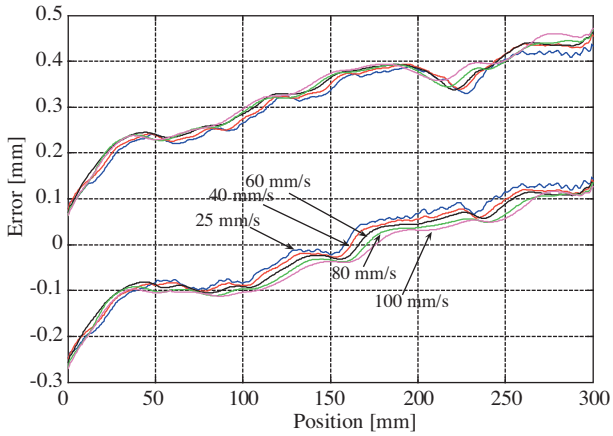

Figure 13. Low-pass filtered displacement errors for various steady-state velocities.

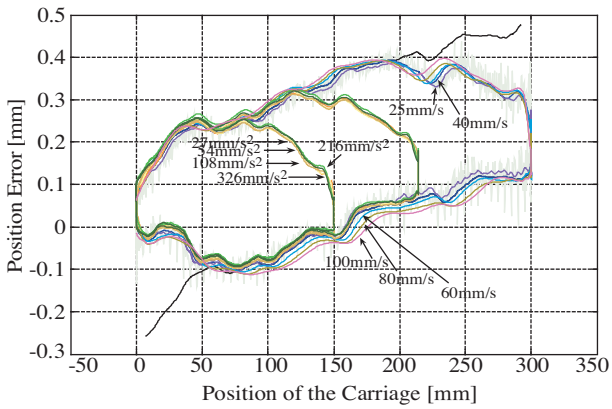

Figure 14. Effect of acceleration/deceleration on displacement errors.

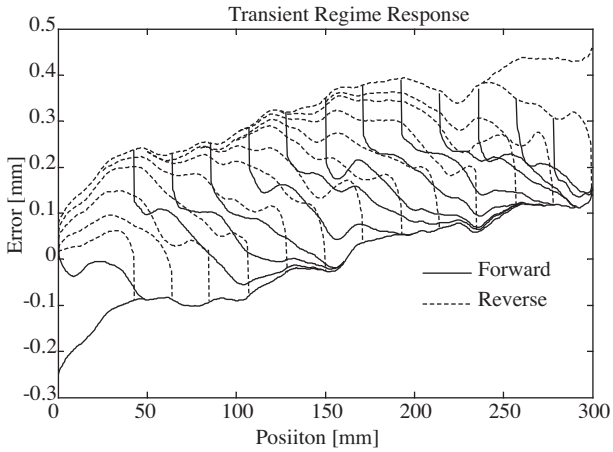

Figure 15. Position errors on motion reversals at various intermediate locations.

5.1. Model 1: Linear transition

First, hysteresis band model shown in the Figure 16 is developed. Depending on the direction of travel x and the position registered when the direction changes, a linear path is traversed inside the band as

$$y(k) = \begin{cases} m \cdot x(k) - h, & x(k) \geq x(k-1) \\ u(k) = y_d(k) - a\left[x(k) - x_d(k)\right], & \left[x(k) \geq x(k-1)\right] \wedge \left[u(k) \geq m \cdot x(k) - h\right] \\ m \cdot x(k), & x(k) < x(k-1) \\ u(k) = y_d(k) - b\left[x(k) - x_d(k)\right], & \left[x(k) < x(k-1)\right] \wedge \left[u(k) < m \cdot x(k)\right] \end{cases} \tag{14}$$

Here, a, b, m denote the value of various lines while h describes the hysteresis band. In this expression, k is time index; $x(k)$ is primary encoder position at $t{=}kT$ while $y(k)$ denotes position error at $t{=}kT$. Note that x_d and y_d corresponds to the primary encoder position and the error, respectively when a change in motion

direction is registered:

$$x_d(k) = \begin{cases} x(k-1), & \{[x(k) \geq x(k-1)] \wedge [x(k-1) < x(k-2)]\} \\ & \vee \{[x(k) < x(k-1)] \wedge [x(k-1) \geq x(k-2)]\} \\ x_d(k-1), & else \end{cases} \tag{15}$$

$$y_d(k) = \begin{cases} y(k-1) - h_g, & \{[x(k) \geq x(k-1)] \wedge [x(k-1) < x(k-2)]\} \\ y(k-1) + h_g, & \{[x(k) < x(k-1)] \wedge [x(k-1) \geq x(k-2)]\} \\ y_d(k-1), & else \end{cases} \tag{16}$$

5.2. Model 2: Exponential transition

As a second alternative, the model in Figure 17 is taken into consideration. In this model, when the motion direction changes, an exponential path is traversed in the loop as

$$y(k) = \begin{cases} m \cdot x(k) - h, & x(k) \geq x(k-1) \\ u(k) = y_d(k) - A\left[1 - e^{a[x(k) - x_d(k)]}\right], & [x(k) \geq x(k-1)] \wedge [u(k) \geq m \cdot x(k) - h] \\ m \cdot x(k), & x(k) < x(k-1) \\ u(k) = y_d(k) + B\left[1 - e^{-b[x(k) - x_d(k)]}\right], & [x(k) < x(k-1)] \wedge [u(k) < m \cdot x(k)] \end{cases} \tag{17}$$

Here *A, B, a, b* denote the parameters of the **exponential** curves while x_d and y_d are as defined in (15) and (16).

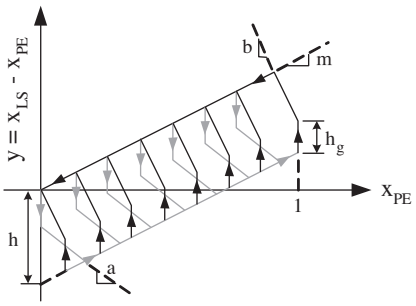

Figure 16. Linear transition model.

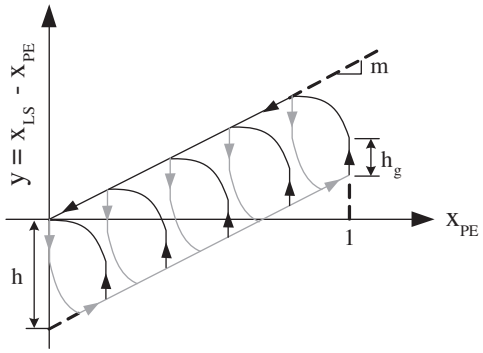

Figure 17. Exponential transition model.

5.3. Model 3: Linear interpolation

As a third and more comprehensive model, a linear interpolation model representing the transitions inside the hysteresis band is considered:

$$y(k) = \begin{cases} \Lambda_f(x(k)), & x(k) \geq x(k-1) \\ u(k) = \Lambda_{ft}(x(k), x(k-1), x_d(k), y_d(k)), & [x(k) \geq x(k-1)] \wedge [u(k) \geq m \cdot x(k) - h] \\ \Lambda_r(x(k)), & x(k) < x(k-1) \\ u(k) = \Lambda_{rt}(x(k), x(k-1), x_d(k), y_d(k)), & [x(k) < x(k-1)] \wedge [u(k) < m \cdot x(k)] \end{cases} \quad (18)$$

where Λ_f, Λ_r indicates the lookup table for the lower and upper band respectively while Λ_{ft} and Λ_{rt} denotes multidimensional lookup tables created using the transient data printed in Figure 15.

6. Results and discussion

These first two models are cross examined and first the free parameters of these models are determined using the relevant experimental data via least squares method. Table 2 tabulates these parameters.

Table 2. Model parameters.

Model	m	h	h_g	a	b	A	B
1: Linear	0.0010594	0.34	0.11	0.0012	0.0012	–	–
2:Exponential	0.0010594	0.34	0.11	-0.05	-0.03	0.07	0.09

With respect to the third (interpolation) model, the relevant parameters are inherited from those of the linear model while two dimensional lookup table which has got a total 650 data points are formed using the characteristic curves in Figure 15.

Once these models and the lookup tables are formed, the estimation performances of all the models are assessed through a complicated scenario where the carriage abruptly changes its motion direction through its course as illustrated in Figure 18. The estimated position error results are presented in Figures 19 through 24. Similarly, Table 3 summarizes the statistics of the resultant data.

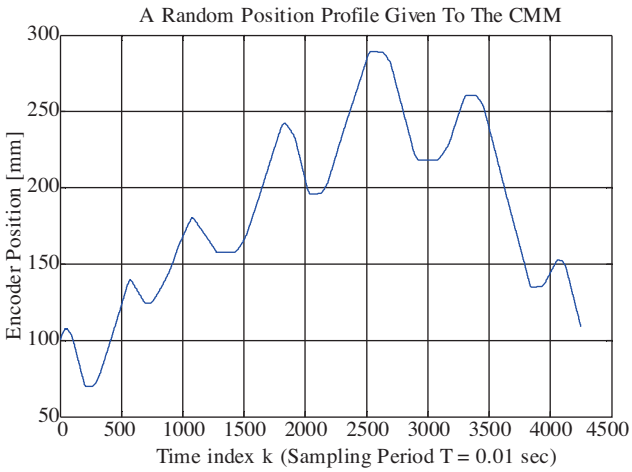

Figure 18. Test scenario.

Table 3. Summary of results.

(μm)	Model 1	Model 2	Model 3	No Model
Max	131	120	99	365
Min	-148	-130	-79	-93
Erms	38	34	26	195

Note that in Table 3, the root-mean-square error is defined as

$$e_{rms} = \sqrt{\frac{1}{K}\sum_{k=1}^{K}\left[x_{LS}(k) - x_{PE}(k) - y(k)\right]^2} \tag{19}$$

The performances of Model 1 and 2 are very close to each other owing to the fact that the fitted curves are quite similar. As expected, linear interpolation yields the best performance because the data which is used to form the lookup tables essentially captures the essence of the transition region.

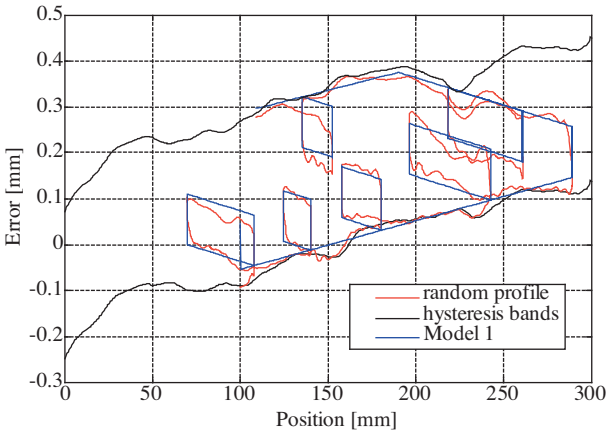

Figure 19. Estimation performance of Model 1.

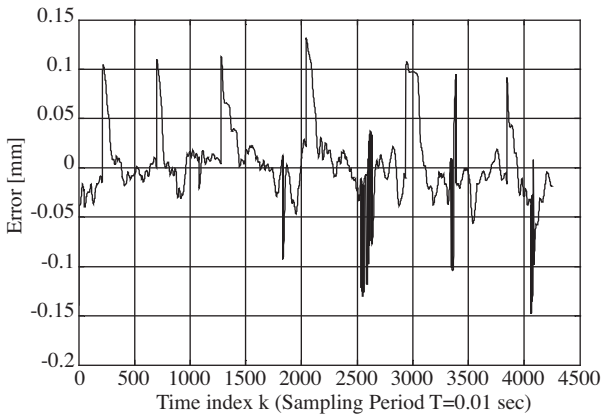

Figure 20. Error profile of Model 1.

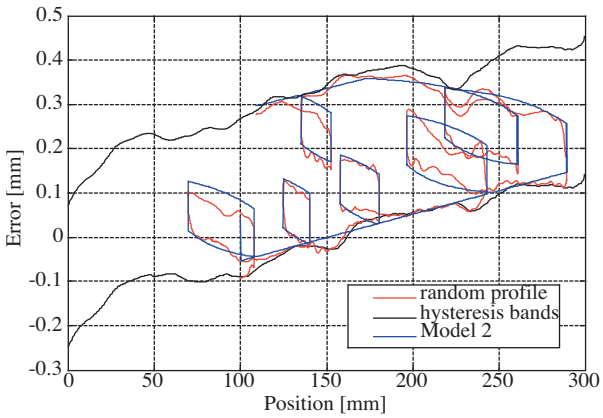

Figure 21. Estimation performance of Model 2.

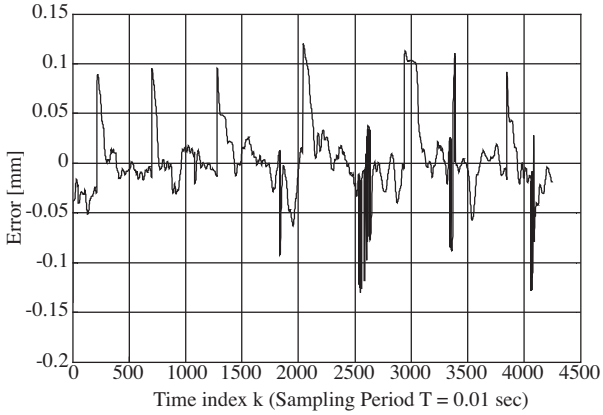

Figure 22. Error profile of Model 2.

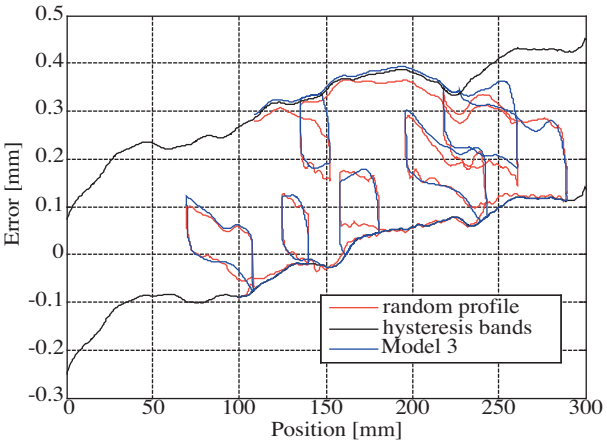

Figure 23. Estimation performance of Model 3.

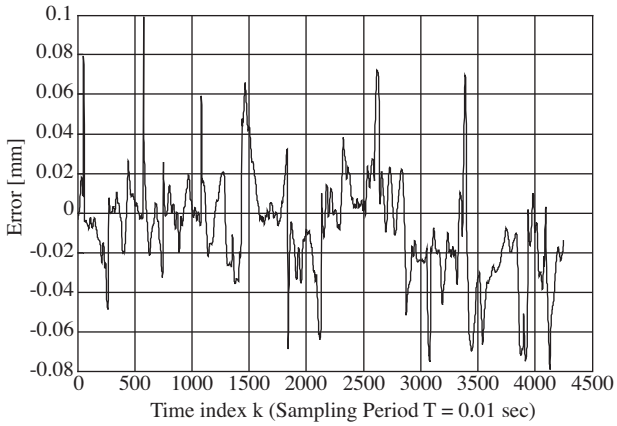

Figure 24. Error profile of Model 3.

7. Conclusion

This study covers some of the important aspects of the timing belt mechanisms that are frequently used in motion control systems. Key points of the paper are:

- Dynamic model of the timing belt drive mechanisms, which could be used in the design of motion control systems, is derived.
- Simulation results, which are based on the developed model, are in a good agreement with the experimental results.
- An experimental study is conducted to investigate the attributes of such mechanisms. During the experiments, extensive data is collected under different operating conditions. The collected data are shown to be both spatially and temporally repeatable in character.
- High repeatability suggests the development (and deployment) of different position estimation / observer techniques.
- A huge error reduction (from 365 micron levels to 30 micron levels) is attained utilizing advanced interpolation methods. The presented techniques, which rely on indirect measurement, bring no additional (hardware) cost to the overall system.
- The paper illustrates that advanced estimation schemes are quite effective when the drive system is not subjected to external loads as well as widely changing operating conditions such as ambient temperature and belt tension.

Acknowledgment

This work has been partially supported by the Turkish Scientific and Technical Research Council (TÜBİTAK) under the project MISAG-257 and partially by METU/BAP under contract

References

[1] A. S. Kulkarni, M. A. El-Sharkawi "Intelligent Precision Position Control of Elastic Drive Systems," IEEE Trans. On Energy. Conv., vol. 16:1, pp 26-31, 2001.

[2] W. Li, M. Rehani, "Modeling and control of a belt-drive positioning table", in *Proceedings of the 22nd IEEE International Conference of Industrial Electronics (IECON)*, vol. 3, Taipei, Taiwan, Aug. 1996, pp. 1984–1989.

[3] Z. Zhao, L. Cai, "On the improvement of tracking performance of positioning tables", in *Proc. of the 22nd IEEE International Conference of Industrial Electronics (IECON)*, vol. 3, Taipei, Taiwan, pp. 1990–1995, 1996.

[4] S. Abrate, "Vibrations of belts and belt drives", *Mechanism and Machine Theory*, vol. 27, no. 6, pp. 645–659, 1992.

[5] D. W. South, J. R. Mancuso, Eds., *Mechanical Power Transmission Components*. New York: Marcel Dekker Inc., 1994.

[6] Firbank, T. C., "Mechanics of the Belt Drive", Int. J. of Mech. Sci., Cilt: 12, s: 1053-1063, 1970.

[7] Özgüven, H.N, Houser, D.R., "Mathematical Models Used in Gear Dynamics – A Review,", *Journal of Sound and Vibration*, vol. 121:3, pp. 383-411, 1988.

[8] Kagotani, M., Ueda, H., Koyama, T., "Transmission Error in Helical Timing Belt Drives (Case of a Period of Pulley Pitch)", *Journal of Mechanical Design, vol. 123(1), pp. 104–110, 2001*

[9] I.D. Mayergoyz, "Mathematical Models of Hysteresis", Springer-Verlag, New York, 1991.

[10] Kam K. Leang, "Iterative Learning Control of Hysteresis in Piezo-based Nano-positioners: Theory and Application in Atomic Force Microscopes", University of Washington, Ph. D. Thesis, 2004.

[11] I.D. Mayergoyz, A. A. Adly, "Numerical Implementation of the Feedback Preisach Model", IEEE Transactions on Magnetics, vol.248, No. 5, 1992

[12] C. Canudas de Wit, H. Olsson, K. J. Astrom ve P. Lischinsky, "A New Model for Control of Systems with Friction", IEEE Trans. on. Automatic Control, vol. 40, pp. 419–425, 1995.

[13] O. A. Bauchau, C. K. Ju, "Modeling Friction Phenomena in Flexible Multibody Dynamics", Comput. Methods App. Mech. Engr., vol. 195, pp. 6909–6924, 2006.

[14] J. J. Choi, S. I. Han, J. S. Kim, "Development of a Novel Dynamic Friction Model and Precise Tracking Control Using Adaptive Back-Stepping Sliding Mode Controller", Mechatronics, vol. 16, pp. 97–104, 2006.

[15] E. Ostertag, M. J. Carvalho-Ostertag, "Fuzzy control of an inverted pendulum with fuzzy compensation of friction forces", *International Journal of Systems Science*, vol. 24, no. 10, pp. 1915–1921, 1993.

[16] Kilic, E., Dolen, M., Koku, B. A., Dogruer, C. U., "Novel Position Estimators for Timing Belt Drives", *Journal of Automation, Mobile Robotics, and Intelligent Systems, vol. 1, no. 2, pp. 55-61, 2007*

[17] B. Armstrong-Helouvry, P. Dupont, C. Canudas De Wit, "A survey of models, analysis tools and compensation methods for the control of machines with friction", *Automatica*, vol. 30, no. 7, pp. 1083–1138, 1994.